Potential existence of post-perovskite nitrides; DFT studies of ThTaN$_3$ ☆

Samir F. Matar *, Gérard Demazeau

CNRS, Université de Bordeaux, ICMCB, 87 avenue Dr Albert Schweitzer, 33600 Pessac, France

ARTICLE INFO

ABSTRACT

Within density functional theory, the equations of state for cubic perovskite (c-pv) and hypothetic orthorhombic perovskite (o-pv GdFeO$_3$-type) and post-perovskite (ppv) forms of ThTaN$_3$ are obtained. The decreasing volume and stabilizing energy indicate pressure enabled transitions: c-pv → o-pv → ppv. From electronic structure analysis the chemical system is found insulating in the c-pv ground state form with ~1 eV band gap and semi-conducting for the ppv due to increased covalence. The chemical bonding properties show that Th and Ta bondings with the 2 N sites are selectively differentiated and reinforced for Ta–N bond within ppv form. This is the consequence of the corner as well as edge sharing octahedra characterizing ppv while pv structures have only corner sharing octahedra. It is the first case of potential post-perovskite nitride.

1. Introduction

The structural transformations of Minerals in deep Geosphere are an important challenge for explaining the structure and the properties of the Earth [1]. Taking into account that MgSiO$_3$ and (Mg,Fe)SiO$_3$ with the perovskite structure as the main components of the lower mantle [2] and due to the seismic anisotropy of the D″ layer at the boundary between the lower mantle and the outer core, the structural transformation of MgSiO$_3$ was investigated by both Oganov and Ono [3] and Murakami et al. [4]. Both research works postulated the transformation of perovskite (pv) to the CaIrO$_3$-type structure, which was then called *post-perovskite* (ppv). The recent stabilizations of the ppv form for CaRuO$_3$ by Kojitani et al. [5], CaPtO$_3$ by Ohgushi et al. [6] and Inaguma et al. [7], CaRhO$_3$ by Shirako et al. [8] have extended the interest of the post-perovskite structure from Geosciences to Materials Chemistry. Through a simple analysis, two main factors seem to play an important role for stabilizing such a ppv structure for ABO$_3$:

- the degree of distortion of the perovskite-precursor (pv) with the GdFeO$_3$-type (corresponding to the tilting of the BO$_6$ octahedra and a small value for the Goldschmidt factor), and
- the covalence of the B–O bond.

Consequently, the ppv structure can be observed for the ABO$_3$ compositions involving a d^4 or a d^5 B element and an A cation such as Ca^{2+}. At the present time, due to the importance of oxides in the Earth mantle, mainly ABO$_3$ compositions have been investigated. However, the ppv structure has been observed for NaMgF$_3$ with the neighborite structure in a pressure range between 28 and 30 GPa by Martin et al. [9]. Such a result opens new horizons for the interest of the ppv structure in materials chemistry. The pv structure (cubic, c-pv and orthorhombic, o-pv) is only characterized by shared corners octahedra and a three-dimensional (3D) network, while the ppv one, shown in Fig. 1, corresponds to a two-dimensional (2D) network where octahedra share both corners and edges. Consequently, compounds with ppv structure can be characterized by specific electronic properties. Recently, the metal–insulator transition observed in Ca$_{1-x}$Na$_x$IrO$_3$ with the ppv structure is an interesting example [10].

Considering the covalence of the B–O bond as a critical factor for stabilizing the ppv structure, nitrides would appear as good candidates for developing novel ppv compounds. The number of nitrides with the perovskite structure is reduced, ThTaN$_3$ being considered as the most known [11]. Therefore, it was important to validate through energy derived quantities from ab initio calculations whether pv-nitrides could adopt the ppv structure and in which conditions. This is herein investigated for the first time in archetype trinitride, ThTaN$_3$ by considering firstly the actual cubic structure; such a structure could be metastable at room temperature conditions due to the high temperature required for preparing ThTaN$_3$ (1400 °C) [11]. Then ab initio parameters for orthorhombic GdFeO$_3$-pv and CaIrO$_3$-ppv are
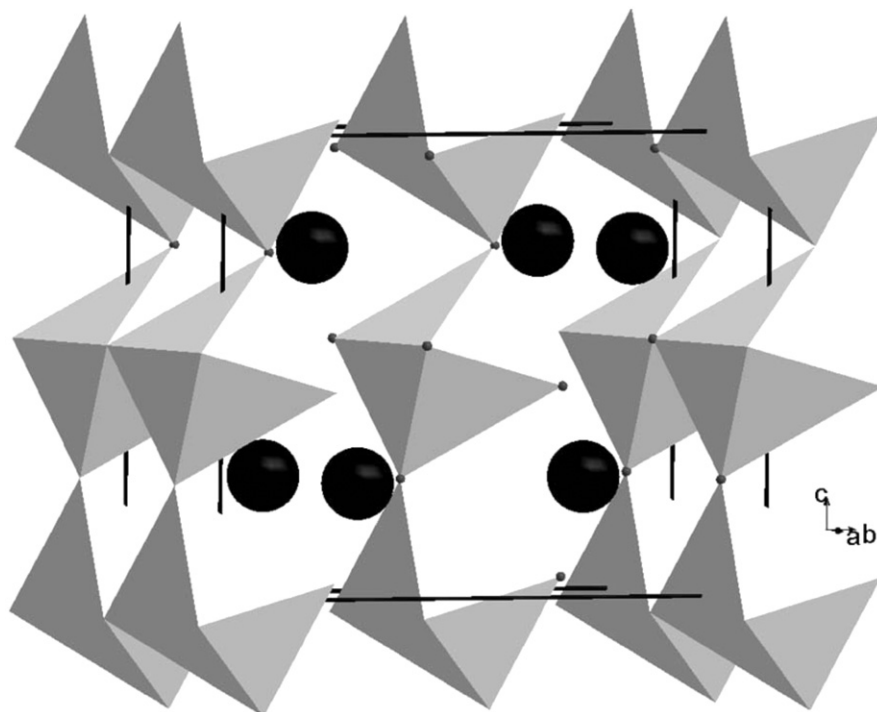
Fig. 1. Arrangement of edge sharing tilted BX_6 octahedra in the *Cmcm* orthorhombic post perovskite structure ABX_3 with $B=$Ta and $X=$N here. Black spheres between the octahedra represent large A (Th) cation. Lattice vectors *a*, *b*, *c* correspond with data in Table 1.

derived, following the factors given above. For this purpose we call for two complementary methods within the well established quantum mechanical framework of the density functional theory, DFT [12,13].

2. Computational methods

A pseudo-potential approach within the VASP code [14,15] is firstly used. Besides testing the calculations in their ability to yield the experimental parameters of ThTaN$_3$ cubic perovskite [11], the method enables optimizing the structure and parameters for hypothetic orthorhombic PV and PPV phases, starting from known oxide systems. This follows from the structural geomimetism principle [16] with Th, Ta and N placed at Ca, Rh and O sites, respectively, in CaRhO$_3$ oxide [8]. Then the respective equations of states (EOS) are obtained to confront the equilibrium volumes and relative stabilities. This is done through energy–volume curves fitted with Birch EOS [17]. For these purposes, pseudo-potentials built within the PAW (projector augmented wave) method [18,19] are used, due to the presence of thorium (5*f*-subshell). For the treatment of the effects of exchange and correlation a local density approximation (LDA) [20] has been adopted. Preliminary test calculations for c-PV with gradient functional GGA [21] potentials led to unfavorable total energy with respect to LDA calculations by ~ 2.8 eV per formula unit (fu). The calculations are converged at energy cut-offs of 500 eV for cubic PV and 400 eV for orthorhombic PV and PPV ThTaN$_3$, respectively, for the plane-wave basis set. The **k**-point integration is carried out with a starting mesh of $4 \times 4 \times 4$ up to $8 \times 8 \times 8$ for best convergence and relaxation to zero strains. The Brillouin-zone integrals are approximated using a special *k*-point sampling following Blöchl [18].

For a full description of the electronic band structures and of chemical bonding, the scalar relativistic all-electrons augmented spherical wave (ASW) [22,23] method is used. Like in the calculations with pseudo-potentials, the exchange and correlation effects are accounted for with an LDA functional [24]. In the ASW method, the wave function is expanded in atom-centered augmented spherical waves, which are Hankel functions and numerical

solutions of Schrödinger's equation, respectively, outside and inside the so-called augmentation spheres. In order to optimize the basis set, additional augmented spherical waves are placed at carefully selected interstitial sites (IS). The choice of these sites as well as the augmentation radii are automatically determined using the sphere-geometry optimization algorithm [25]. Self-consistency is achieved by a highly efficient algorithm for convergence acceleration [26]. The Brillouin zone integrations are performed using the linear tetrahedron method with up to 1728 and 1469 **k**-points for cubic and orthorhombic phases, respectively [18,23]. In the minimal ASW basis set, we have chosen the outermost shells to represent the valence states using partial waves up to $l_{max.}+1=4$ for Th, $l_{max.}+1=3$ for Ta and $l_{max.}+1=2$ for N and IS. The completeness of the valence basis set is checked for charge convergence. The self-consistent field calculations are run to a convergence of $\Delta Q = 10^{-8}$ for the charge density and the accuracy of the method is in the range of about 10^{-8} Ryd (1 Ryd $= 13.6$ eV) regarding energy differences.

The relative magnitude of the chemical bonding is obtained based on the overlap population analysis: S_{ij}, *i* and *j* being two chemical species. The crystal orbital overlap population (COOP) [27] criterion is used as implemented within the ASW method [23]. For the purpose of establishing trends of chemical bonding strength, we show the integrated COOP (*i*COOP): below the curves, a larger area indicates a larger bonding. In the plots positive, negative and zero *i*COOP magnitudes indicate bonding, anti-bonding and non-bonding interactions, respectively.

3. Equation of state and charge density

3.1. Geometry optimization and equation of state

The results of full geometry relaxation for cubic and orthorhombic perovskites, resp. c-PV o-PV, and base centered orthorhombic PPV ThTaN$_3$ are presented in Table 1. The optimized cell volume for c-PV shows a good agreement with experiment with a slightly smaller